Electrical Engineering
https://doi.org/10.1007/s00202-020-01157-6

ORIGINAL PAPER

Cascaded HVDC gaseous circuit breaker performance using black box arc model

Osama E. Gouda[1] · Ghada Amer[2] · Mohamed Awaad[2] · Manar Ahmed[2]

Received: 7 April 2020 / Accepted: 12 November 2020

Abstract
The development of renewable sources of electrical energy represents the main goal of the most countries. This energy has to be transmitted for a long distance for the utilization in populated areas. The need of high-voltage direct current circuit breakers represents the key of the development of high-voltage direct current transmission systems. High and extra high-voltage six sulfur hexafluoride circuit breakers need more than one interrupter to *be* stable during arc extinguishes*, so* it can be used in high-voltage systems as cascaded interrupters. In this article, the multi-break high-voltage direct current HVDC gaseous circuit breaker characteristic is investigated by employing Mayr and Cassie arc models. The influences of the models parameters on the arc interruption time are studied using MATLAB/Simulink program. It is concluded that the simulated results by employing black box arc models achieve a success in multi-break HVDC gaseous circuit breakers simulation. Employing BBAMs black box arc models has proved more flexibility to study the effect of different controlled and uncontrolled parameters on the multi-break high-voltage direct current gaseous circuit breaker HVDCGCB arcing time. That has proved more flexibility to study the effect of different controlled and uncontrolled parameters on the arcing time. The main contributions of this article in points can be summarized as employing black box arc models achieves a success in multi-break HVDC gaseous circuit breakers simulation, investigation of the influence of commutation parameters on the cascaded HVDC gaseous circuit breaker interrupter performance, the controlled and uncontrolled parameters affecting the arcing time of HVDCGCB has been studied, the impact of the fault resistance value on arcing time and the damping resistance influence on the transient recovery voltage are investigated, and additionally, the initial transient interruption and the Metal Oxide Varistor voltages are analyzed. From the investigated forty cases done to check the Mayr's model validity in the HVDC CD simulation, it is found that the values of P and τ which give acceptable outputs are at $\tau = 10^{-6}$ s, and P in range of 10^7 W to 10^{11} W. The output of the case $\tau = 10^{-6}$ s, $P = 10^{10}$ W, which is introduced in the paper has proved that when τ reached to 10^{-7} s the MOV current rises and drops and thereafter rises and gradually decreases. This may leads to CB failure Com parameters influence on the interrupter performance are investigated and proved good simulation of the gaseous circuit breaker interrupter.

Keywords Gaseous circuit breakers · Black box arc models · Transient recovery voltage · The arc time constant

Abbreviation

AC	Alternating current
ACZC	Artificial current zero crossing
BBAMs	Black box arc models
BCB	Back-up CB
CBs	Circuit breakers
Com	Commutation
DC	Direct current
EMR	Electromagnetic repulsion actuators
HVDCGCB	High-voltage direct current gaseous circuit breaker
HVDC	High-voltage direct current
HVDCCB	High-voltage direct current circuit breaker
HVDCVCB	High-voltage direct current vacuum circuit breaker
LGSCF	Line to ground short circuit fault
MCB	Main Circuit Breaker
MVDC	Medium-voltage direct current
MOV	Metal Oxide Varistor
PAMs	Physical Arc Models

✉ Osama E. Gouda
prof_ossama11@yahoo.com

[1] Faculty of Engineering, Cairo University, Giza, Egypt

[2] Faculty of Engineering, Benha University, Benha, Egypt

Published online: 02 January 2021

PM	Permanent magnet
$Q(t)$	Stored energy content of the arc column
R	Switching resistance
RRRV	Rate of Rise of Transient Recovery Voltage
SF_6	Six Sulfur hexafluoride
TRV	Transient Recovery Voltage
P	Cooling factor
VDCCB	Vacuum Direct Current Circuit Breaker
g	The nonlinear arc conductance
i	The arc current
U_C	The steady-state arc voltage
u	The arc voltage
$v(t)$	Instantaneous arc voltage
$i(t)$	Instantaneous arc current
τ	The arc time constant

1 Introduction

As it is known, the DC transmission has more advantages than the alternating current AC transmission, such as low power losses, low cost and higher efficiency. In Ref. [1] coordinated operation for network riding through DC fault has been investigated. References [2, 3] carried out modeling of high-power hybrid DC circuit breaker for grid level. In the next years, the DC transmission will achieve a virtual excess in connecting the renewable energy sources with the standard grid [4]. Multi-terminal medium-voltage DC grids fault location and isolation are investigated by Ref. [5]. There is major advantage of the DC transmission that is mainly used in connection between asynchronous AC grids over large distances. HVDC circuit breakers for HVDC grid applications are studied in Ref. [6]. References [7, 8] reported a study on HVDC circuit breakers for HVDC grid applications. The interruption process of the DC fault is very complex due to the absence of the natural current zero crossing which is not the case in the AC. A Review on HVDC Circuit Breakers is done by Mokhberdoran et al. [9]. Passive and active DC Breakers in HVDC Project are investigated in [10]. Classification of fault clearing strategies for HVDC grids is presented in [11]. Reference [12] summarized the models of medium-voltage DC vacuum circuit breaker. The absence of the natural current zero crossing in the DC network makes a problem in the growth of HVDC CBs. Hence, to interrupt the HVDC CB arc, it is required to add supplemental components to traditional AC CB to make an artificial current zero crossing (ACZC). Reference [13] studied the arcing time of a DC circuit breaker based on superconducting current-limiting technology applied superconductivity using Mayr's model. Reference [14] carried out comparative evaluation of power loss in HVAC and HVDC transmission systems. Reference [15] suggested circuits for HVDC circuit breakers testing. Reference [16] carried out enhancement of commutation circuit design of HVDCCB using EMTP and the CB arc is modeled using the modified Mayr equations with using active Com circuit. Reference [17] investigated the parameters affecting the arcing time of HVDC circuit breakers using black box arc model. Thus, many authors suggested employing active and passive commutation types. A novel solid-state circuit breaker for on-board DC micro-grid system is investigated by Ref. [18]. Development of a novel HVDC circuit breaker combining liquid metal load commutation switch and two-stage commutation circuit is carried out by Win et al. [19]. Methodology of DC breaker based on discrete metal oxide varistors with series power electronic devices for HVDC application is presented in Ref. [20]. Mixed gas DC circuit breaker with superconducting fault current-limiting technology is investigated by Ref. [21]. Quench and Recovery Characteristics of Solenoid and Pancake superconducting fault current limiter (SFCL) under DC Impact Current are discussed by Ref. [22].

Many efforts are directed to explain the arc behavior in the DC arc models [23]. Traditional arc models are divided into two groups, physical arc models and black box arc models (BBAMs). Physical arc models cannot be used to describe the dynamic arc model because of mathematical issues [23]. On the other hand, the BBAM is the most suitable model to characterize the arc behavior [17]. It describes the external electrical features of the arc [23]. It states the changing of the arc nonlinear conductance with time. HVDCCB composes of a commutation (Com) branch, connected in parallel with the main circuit breaker (MCB) which is in parallel with the metal oxide varistor (MOV) [24]. The Com branch is composed of a pre-charged Com capacitor C, a Com inductance L and a Com switch S [20, 25]. The Com branch generates an oscillating current which superimposed on the current in the MCB in the interruption process [26]. The MOV is employed to clip the voltage across the MCB during interruption and to absorb the stored energy in the DC line inductances [27–29]. Some models utilize Back-up CB (BCB) in the DC source side to interrupt the residual current after interruption process [30, 31]. The HVDCVCB was simulated by electromagnetic repulsion actuators (EMR) only as in [20], or by a mechanism operated by EMR principle as in [25], or by a mechanism mixed of two systems EMR and a permanent magnet (PM) system as in [32].

Reference [33] suggested mechanical DC circuit breaker model for real-time simulations. Modifications are done on Mayr's arc model by Ref. [34]. Arcing time of a DC circuit breaker based on a superconducting current-limiting technology is investigated by Wang et al. [35]. A review identifying future research needs for HVDC circuit breakers is done by [36]. Reference [37] presented a range of scenarios and testing circuit for evaluating and comparing the performance of HVDCCB models. Reference [38] presents a novel technique

for artificial current zero SF6 DC circuit breaker charging by superconducting voltage.

In this paper, HVDCG CB model is introduced by applying Mayr and Cassie BBAM to characterize the arc behavior. It is concluded that the simulated results by employing black box arc models achieve a success in multi-break HVDC-CBs simulation. Effects of Com parameters on the interrupter performance are also investigated. The effect of commutation parameters on the multi-break HVDC gaseous circuit breaker interrupter performance and the impact of the changing of fault resistance value on arcing time are discussed. The damping resistance influence on the transient recovery voltage is also investigated. Additionally, the initial transient interruption metal oxide varistor voltages are analyzed.

2 Theoretical background

Dynamic arc equation is assumed to describe the dynamic characteristics of the arc depending on the energy conservation principle. The arc is usually exposed to heating from the electrical power injects in the arc, and dissipating power by cooling, if the heating power is larger than the power dissipation, the energy content in the arc column will increase and vice versa. Differential equation can be deduced depending on this hypothesis, in addition to applying further assumptions [24, 39, 40].

2.1 Mayr's arc model

Mayr's model is used to define the arc conductance variation in time as a function of electrical power loss in the arc. Mayr's model dynamic arc equation can be used to define the arc behavior with the following assumptions [24].

- The arc column cross section area and length keeps constant.
- The arc column temperature changes in time exponentially.
- The power dissipation in arc column keeps constant.
- The arc column temperature and conductivity follow the changes in current, in order to remain constant power dissipation.

As mentioned in [40], Mayr's dynamic arc equation can be deduced from the energy balance equation, where Q is the stored energy content of the arc column, which results from the imbalance between heating power and cooling power, P_H is the heating power resulting from the electrical power that inters the arc and P_C is the cooling power resulting from the power dissipated by the arc. The equation of the arc power balance is

$$\frac{\mathrm{d}Q}{\mathrm{d}t} = P_{\mathrm{H}} - P_{\mathrm{C}} \tag{1}$$

By further assumption that the cooling power P and arc conductance $g(Q)$ are arbitrary functions of Q, according to [24], the arc conductance $g(t)$ relies on the stored energy content $Q(t)$.

$$g(t) = K_{\mathrm{H}} \frac{Q(t)}{P\mathfrak{C}} \tag{2}$$

$\mathfrak{C}$ is the arc time constant. By re-forming Eq. (1) and substituting Eq. (2), the dynamic arc equation is represented as follows [39]:

$$\frac{\mathrm{d}Q}{\mathrm{d}g}\frac{\mathrm{d}g}{\mathrm{d}t} = P_{\mathrm{H}} - P_{\mathrm{C}} \tag{3}$$

where $P_{\mathrm{H}} = v(\mathrm{t})i(t)$ and P_C is constant equals P, after simple algebraic handling, Eq. (3) equates into the Mayr's equation

$$\frac{P\mathfrak{C}}{g}\frac{\mathrm{d}g}{\mathrm{d}t} = v(t)i(t) - P \tag{4}$$

The dynamic of the arc conductance can be represented by the following differential Eq. (5), which is the general form of Mayr's dynamic arc equation

$$\frac{1}{g}\frac{\mathrm{d}g}{\mathrm{d}t} = \frac{1}{\tau}\left(\frac{gu^2}{p} - 1\right) \tag{5}$$

where g is the nonlinear arc conductance, $g = \frac{u}{i}$, u is the arc voltage, i is the arc current, and τ is the arc time constant and P is cooling power coefficient

It is obviously clear that Mayr's model uses two parameters to apt the dynamic arc characteristics versus experimental data. Those parameters are cooling power coefficient (P) and arc time constant ($\mathfrak{C}$).

2.2 Cassie arc model

A.M. Cassie introduced his first differential arc equation that describes the arc behavior and the changes in the arc conductance due to thermal process that takes place inside the arc. As the electrical arc current is generated generally due to the convection loss in the high current area, it is not suitable near to the current zero crossing point and it behaves like an independent voltage generator when it reaches to the steady-state arc voltage [41]. It is noteworthy that, the Cassie arc model can be used in an area away from current zero crossing, and near to high current area. The arc characteristics are defined by Cassie with the following assumptions.

- The arc column has the form of a cylinder filled with highly ionized gas and free electrons.
- Arc cylindrical column with uniform temperature and current density, but its diameter is altered in time and embrace the change in current.
- During the arc process the arc voltage is constant.
- The power dissipation is assumed to be proportional to the column cross section area.

As mentioned in [20, 41] these assumptions were verified experimentally. A linear relation is deduced between arc conductance and energy storage capacity of arc to present Cassie dynamic arc equation.

$$\frac{1}{g}\frac{\mathrm{d}g}{\mathrm{d}t} = \frac{1}{\mathfrak{C}}\left(\frac{u^2}{Uc^2} - 1\right) \tag{6}$$

where $\mathfrak{C}$ is the arc time constant, g is the arc conductance (i/u), u is the arc voltage and U_C is the steady-state arc voltage.

3 Cascaded HVDCGCB model description

The multi-break HVDCGCB given in Fig. 1a comprises three cascaded interrupters of DCCB; each interrupter is connected in parallel with R_1C_1 branch. This branch is used to control the rate of rise of transient recovery voltage. The second one is the Com branch. It includes Com capacitance (C), Com inductance (L) and Com switch (S) to generate an oscillating current which superimposed on the current in the MCB in the interruption process. The third parallel branch is the MOV branch which is a metal-oxide surge arrester having an extreme nonlinear voltage–current characteristic, which is described as:

$$I_{\mathrm{MOV}} = K_{\mathrm{MOV}} V_{\mathrm{MOV}}^{\alpha} \tag{7}$$

K_{MOV} is a constant and α is nonlinearity exponent reliant on the operating region of the MOV. It is employed to clip the voltage across the HVDCCB during interruption and to absorb the stored energy of the DC line inductance after the arc interruption.

The system parameters are similar to that reported by Ref. [32]. The DC supply is considered to be 110 kV, the rated current is 2 kA, the short DC line parameters are ($R_0 = 1.746\ \Omega$, $L_0 = 50.6$ mH), load resistance $R = 53.254\ \Omega$. The MCB comprises a number of modules in series and each one has a gaseous DC interrupter and R_1C_1 snubber branch. For 110 kV DC system, the main circuit breaker composed of three GDCB modules.

This paper, suggested using black box arc model (BBAM) in the HVGDC interrupter module employing Mayr and Cassie models. The R_1C_1 branch is used for damping of the rate of rise of the transient recovery voltage. Its parameters are taken as $R_1 = 100\ \Omega$, $C_1 = 5000$ pF. The MOV branch protection voltage is considered to be 165 kV. In the Com branch, the pre-charged voltage of the C is 20 kV and its parameters are chosen to be $C = 9.53\ \mu$F and $L = 26.53\ \mu$H.

In this paper, the Com branch parameters are changed to study their effect on the Com current, the transient recovery voltage, the interrupting time and MOV branch current and voltage.

It has to be noticed that the Com branch is only used in the Mayr model, and it is not used in the Cassie model. As in the Cassie model, the interruption process is only demanded to investigate the steady-state arc voltage over source voltage to reduce the system current rapidly to zero.

4 Simulation of cascaded HVDC gaseous circuit breaker

4.1 Simulation using Mayr's model

Plenty of models can be considered to simulate the arc of interrupter of HVDCGCBs; in the authors' opinion Mayr and Cassie models have been chosen from point of view their simplicity and at the same time they give reliable results. In this paper Mayr and Cassie BBAMs are employed to simulate the arc model in three cascaded gaseous interrupters. The DC fault modeling simulated using MATLAB/Simulink Mayr BBAM simulation is given in Fig. 1b.

To check the validity of using Mayr's model in the HVDC CB simulation, the parameters of Mayr BBAM, p and τ, are changed. Forty cases are investigated to check the validity of the method; two of them are given in Table 1. The system operation sequence of the HVDCGCB using Mayr model is demonstrated as following:

(1) The operated normal current $I_{\mathrm{rated}} = 2$ kA.
(2) The line to ground short circuit fault (LGSCF) occurs at 7 ms.
(3) The fault is detected when the current in MCB interrupters increased and the MCB interrupters open.
(4) The Com switch S closes at 10.09 ms to connect the Com branch which is in parallel with the MCB. The Com LC circuit produces a high-frequency oscillating current to be superimposed on the current in the MCB and its amplitude increased to create a current zero-crossing.
(5) As soon as, the current in the MCB reaches zero, the arc is extinguished and TRV happens.
(6) After the capacitance (C) discharges the voltage across it becomes zero, and the capacitance starts to be charged reversely. The charged voltage of the capacitance (C) rises quickly, and then TRV between the MCB contacts lasts to rise. It reaches to the protection voltage of MOV.

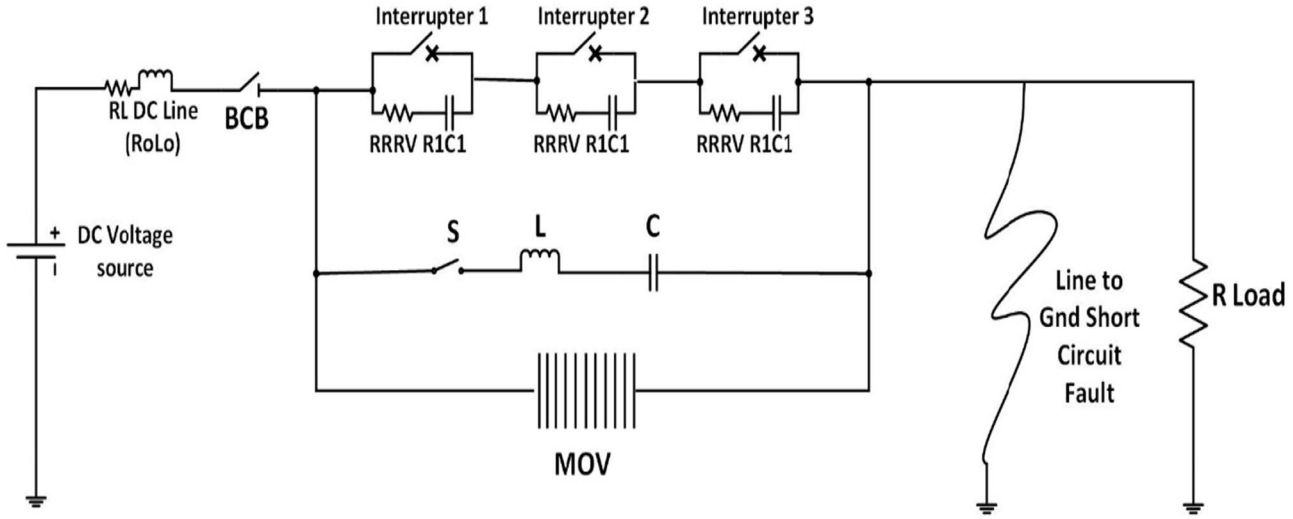

(a)

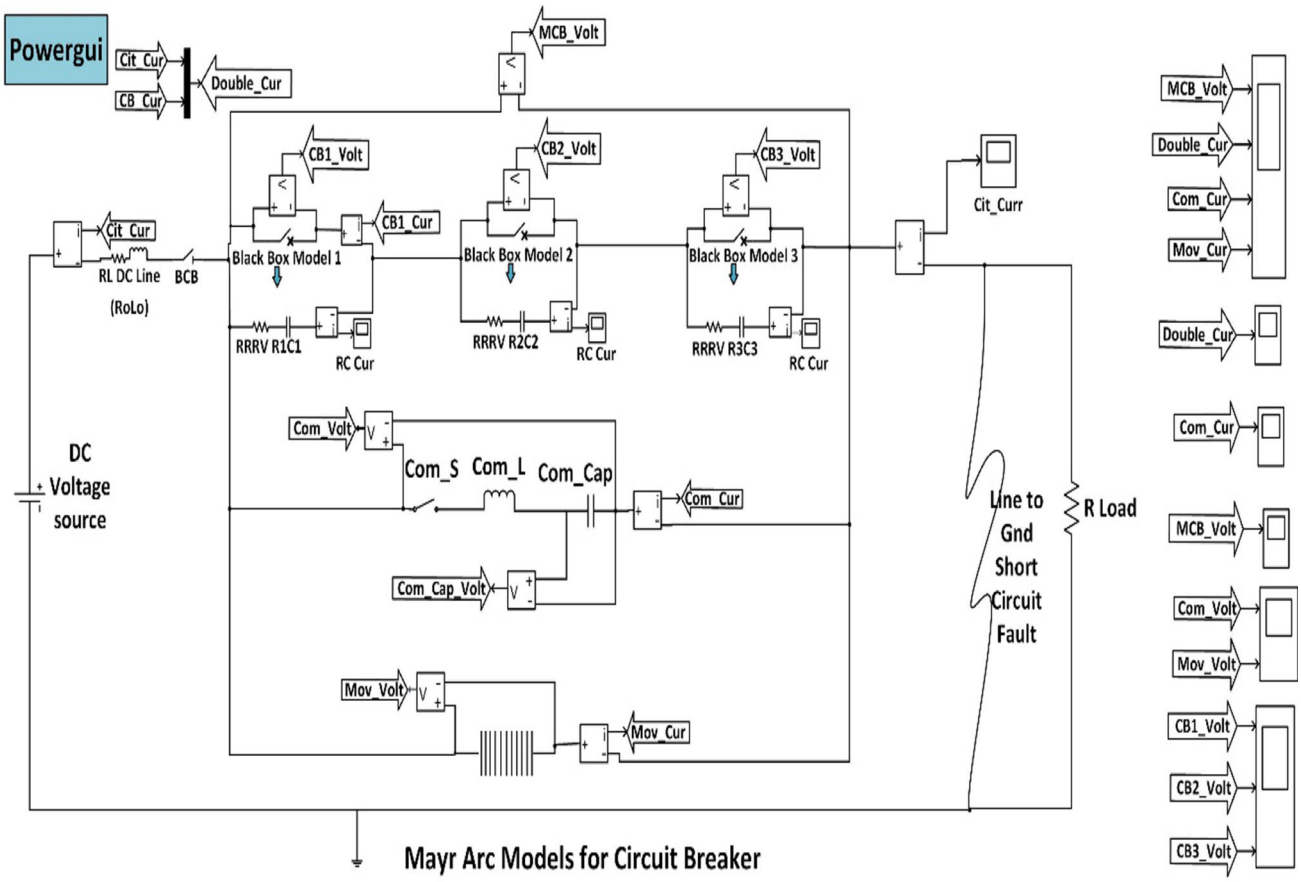

(b)

Fig. 1 High-voltage direct current circuit breaker model and Mayer simulation, **a** circuit breaker model, **b** Mayer BBAM simulation

(7) Then, the current begins to flow through the MOV branch and the MOV starts to absorb the energy remained in the system inductances.

(8) As soon as the MOV absorbs this energy, the fault is cleared.

Table 1 Examples of the calculations contain samples of the simulation system current (kA), CB current (kA), Com current (kA) and MOV current (kA)

Case number	Comparison	Mayr's model				
		System current (kA)	CB current (kA)	Com current (kA)	MOV current (kA)	System voltage (kV)
1	$\tau = 10^{-7}$ s, $p = 10^{9}$ W, $R_1 = 100\ \Omega$, $C_1 = 5000$ pF, $C = 9.53\ \mu$F, $L = 26.53\ \mu$H, no BCB					
	Max value	6.483 kA	6.477 kA	6.674 kA	6.673 kA	182.8 kV
	Oscillations	No	No	No	No	Yes
	Arc interruption time	1st zero: 7.12 ms, 2nd zero: 9.30 ms, 3rd zero: 11.50 ms				
2	$\tau = 10^{-6}$ s, $p = 10^{11}$ W, $R_1 = 100\ \Omega$, $C_1 = 5000$ pF, $C = 9.53\ \mu$F, $L = 26.53\ \mu$H, BCB exists and opens at 14 ms					
	Max value	6.600 kA	6.714 kA	6.592 kA	6.626 kA	182.7 kV
	Oscillations	No	No	No	No	No
	Arc interruption time	7.24261 ms				

4.2 Effect of commutation parameters on the interrupter

To study the performance of the commutation circuit parameters on the HVDCGCB interrupter, the C and L are changed as given in the following two cases one when $\tau = 10^{-7}$ s and the other when $\tau = 10^{-6}$ s.

4.2.1 Case 1: $\tau = 10^{-7}$ s, $p = 10^{9}$ W, $R_1 = 100\ \Omega$, $C_1 = 5000$ pF, $C = 9.53\ \mu$F, $L = 26.53\ \mu$H

From the investigated forty cases, the output of cases at $\tau = 10^{-7}$ s, and P in range of 10^{7} W to 10^{11} W is not acceptable, as it causes a sudden increase in the CB voltage, and in the MOV current when CB opens its contacts. This sudden increase may cause damage to CB interrupters. The case of $\tau = 10^{-7}$ s, $P = 10^{9}$ W, which is mentioned in Fig. 2 is one sample of the unacceptable output. When τ reached to 10^{-7} s the MOV current rises and drops and there after rises and gradually decreases as given in Fig. 2d. This may lead to CB failure. It did not happen when $\tau = 10^{-6}$ s. Such this phenomenon cannot be observed in the direct current gaseous circuit breaker testing because of its high value of the CB time constant. This example was added in the article to attract attention to this phenomenon. When the CB opens its contacts, the CB current drops to zero directly as in Fig. 2a, the system current is reduced by small value, the MOV current began to oscillate as presented in Fig. 2c and the breaker voltage oscillates also as shown in Fig. 2d. This may lead also to CB failure.

4.2.2 Case 2: $\tau = 10^{-6}$ s, $p = 10^{11}$ W, $R_1 = 100$, $C_1 = 5000$ pF, $C = 9.53\ \mu$F, $L = 26.53\ \mu$H, BCB exists and opens at 14 ms

The I_{system}, I_{CB}, I_{Com}, I_{MOV} and V_{CB} values are in acceptable range as given in Fig. 3, as shown in this figure there are no oscillations in all currents and breaker voltages.

As it is known the time constant of SF_6 is very short, the circuit breaker model is tested at low values of CB time constant. A lot of calculations have been made to check the validity of Mayr's model in the HVDC CD simulation. The parameters of Mayr's BBAM, P and τ are changed. Forty cases are investigated, the values of P and τ which gave acceptable outputs are at $\tau = 10^{-6}$ s, and P in range of 10^{7} W to 10^{11} W. For example, the output of the case $\tau = 10^{-6}$ s, $P = 10^{10}$ W is the same output in case of $\tau = 10^{-6}$ s, $P = 10^{11}$ W with no BCB.

As mentioned before when τ reached to 10^{-7} s the MOV current rises and drops and thereafter rises and gradually decreases as given in Fig. 2c. This leads to a rapid increase in the circuit breaker voltage followed by drop to zero and thereafter rapid increase again as given in Fig. 2d. This phenomenon is happened in Microseconds μs and may lead to CB failure. It did not happened when $\tau = 10^{-6}$ s. This phenomenon cannot be observed in the circuit breaker testing because of the high value of the CB time constant. Example of case one was added in the article to attract attention to this phenomenon.

In the above two cases given in Table 1 the cooling power factor and the arc time constant are kept fixed. By change of the Com capacitor C and Com inductance L values, the oscillation frequency of the Com current can be calculated according to the relation given in Eq. (8)

$$f_{\text{osc}} = \frac{1}{2\pi\sqrt{LC}} \tag{8}$$

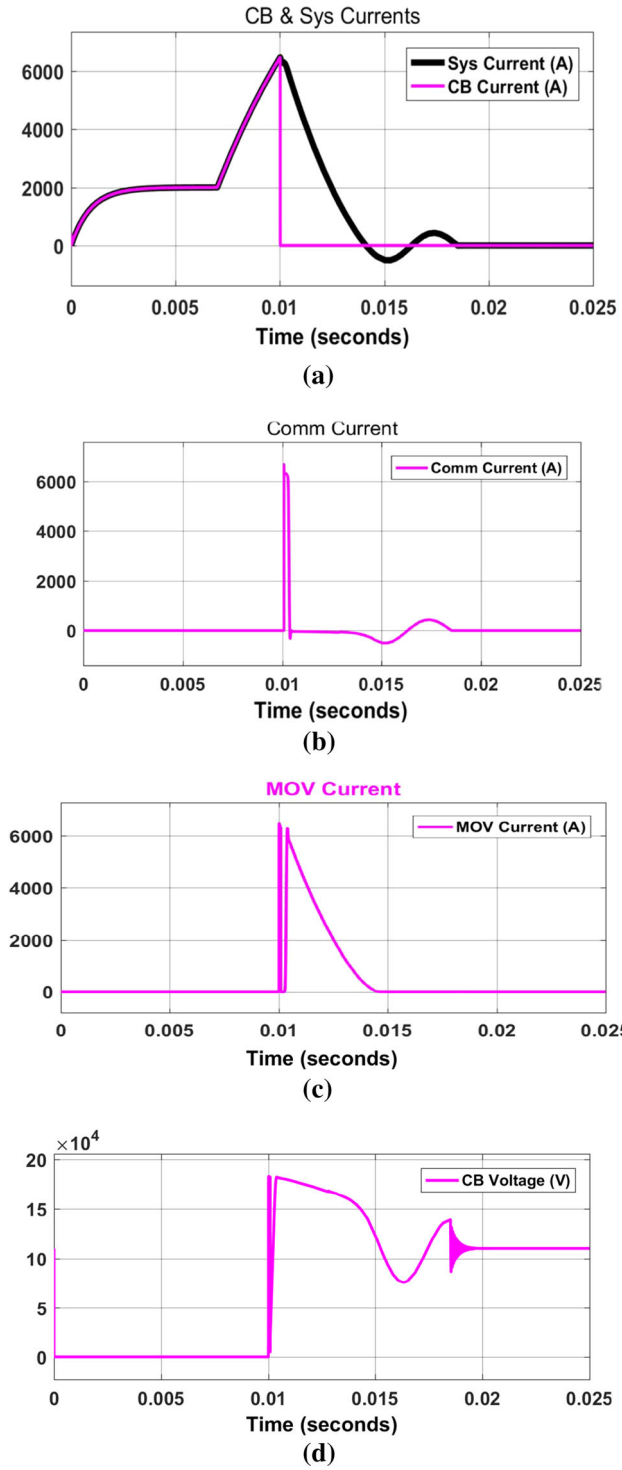

Fig. 2 Mayr outputs for case 1, $\tau = 10^{-7}$ s, $p = 10^9$ W, no BCB, **a** CB and system currents **b** Com current, **c** MOV current, **d** CB voltage

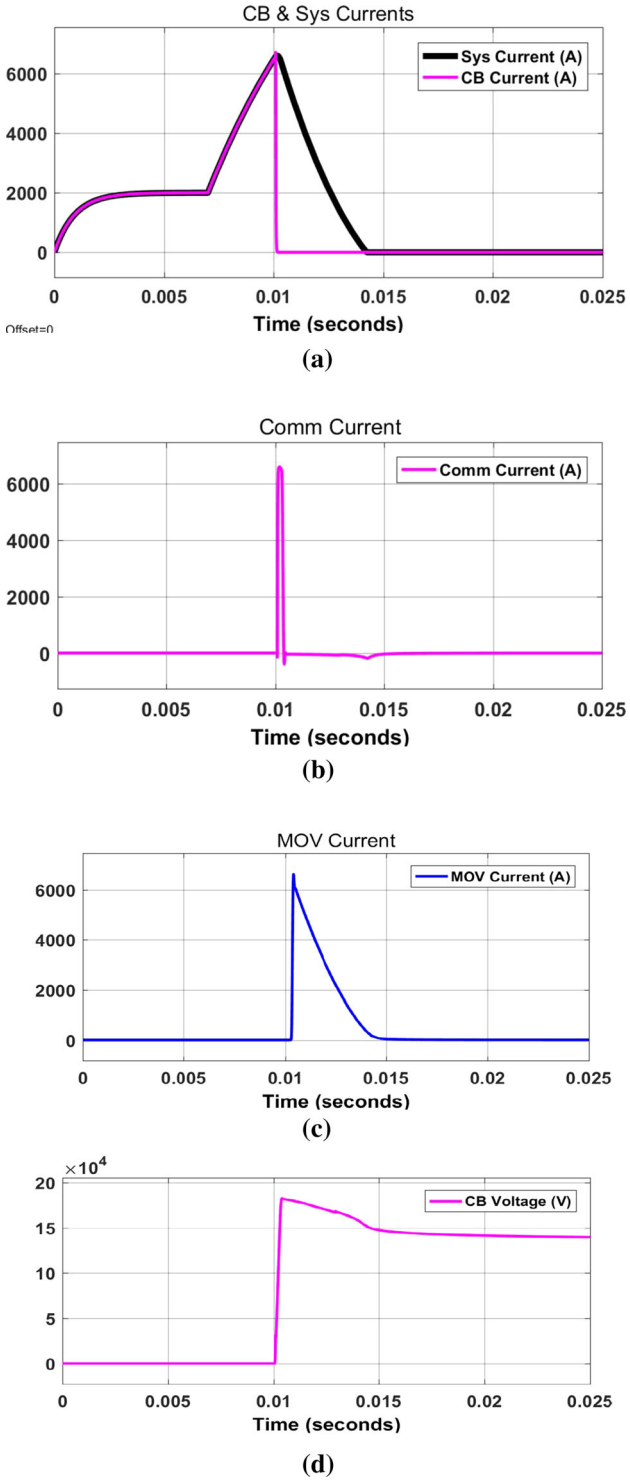

Fig. 3 Mayr outputs case 2, $\tau = 1$ μs, $p = 10^5$ MW and BCB exists and separates at 14 ms, **a** CB and system currents **b** Com current, **c** MOV current, **d** CB voltage

The charging voltage of the Com capacitance C varies according to the relation given in Eq. (9)

$$V_{\text{charging}} = I_c \sqrt{L/C} \tag{9}$$

Figure 4 gives the relations of the Com current (I_c), system current, MOV voltage and MOV current versus time at different frequencies. As it is known the short-circuit fault has to

be interrupted during a specific period of time, from Fig. 4 it is noticed that if the frequency of Com current is too low, the interruption time will be extended and may not be able to face the requirement for arc interruption. It is observed also from Fig. 4a that reducing the Com current frequency increases the time of flow of high current. As example short circuit current of 6.562 kA stays about 0.6 ms at $f_{\text{osc}} = 3.68$ kHz in comparison with 0.1 ms at 71.18 kHz. This may cause damage to the commutation switch. It can be noticed from this figure also that the rate of current changes with time (di/dt) at low frequencies is lower comparing with similar values in case of high frequencies. From Fig. 4b it is observed that the system current slowly reaches the current zero, this means that the fault current will be interrupted in a long time. Also, the MOV voltage lasts for a long time as shown in Fig. 4c and its current peak value is slightly decreases as shown in Fig. 4d. On the other hand if the frequency of the Com current is high, the value of (di/dt) near the zero current period may to be large, this may cause failure of the gas interrupter. The commutation switch should withstand high current within the conduction period. In this interval, the switch of Com circuit is wearing out by the arc. If the corrosion is too significant, it may be possible to damage the Com switch or decreases its achievements.

It has to be noted that with regular increase in the Com capacitor, the rising rate of TRV reduces, which will benefit the dielectric recovery of the MCB after the arc extinguishment. Also, with the rise of Com capacitor, the peak voltage of Com capacitor and MOV is reduced, also the oscillation decreases which reduces the design requirement of the commutation branch and MOA branch. Therefore, a larger Com capacitor with smaller Com inductance and lower charging voltage will improve the interruption capacity, so that the oscillations of 22.5 kHz are realistic.

Figure 5 shows relations of the commutation branch Com voltage, the Com capacitance voltage and MOV voltage at different values of Com capacitance. From Fig. 5a it is noticed that, with the increase in the Com capacitance, the rate of rise of the transient Com voltage decreases. This helps the CB interrupter for the dielectric recovering after the arc extinguish. It can be observed that, with the increase in the Com capacitor, the Com capacitor voltage given in Fig. 5b and the MOV voltage shown in Fig. 5c are decreased, leading to reduction in the design requirements of the HVDCGCB. Finally increasing the Com capacitors with small values of inductances leads to lower charging voltage, improves the HVDCGCB interruption capacity and reduces its dimensions due to the decrease in the required insulation level.

To investigate the inductance variation influences on the behavior of the Com capacitor, the MOV and the commutation voltages, the inductance of the commutation branch is changed from 1 μH as given in Fig. 5a–c to 0.001 μH for Fig. 6a–c. From these figures it is observed that the reduction in the Com inductance has no significant effects on the Com, capacitor and MOV voltages, but it may affect the arcing time. Relationships of the arcing time and cooling power coefficient versus the arc time constant are given in Fig. 5d. The intersection point of the two curves represents the lowest values of P and τ for the Gaseous interrupter design.

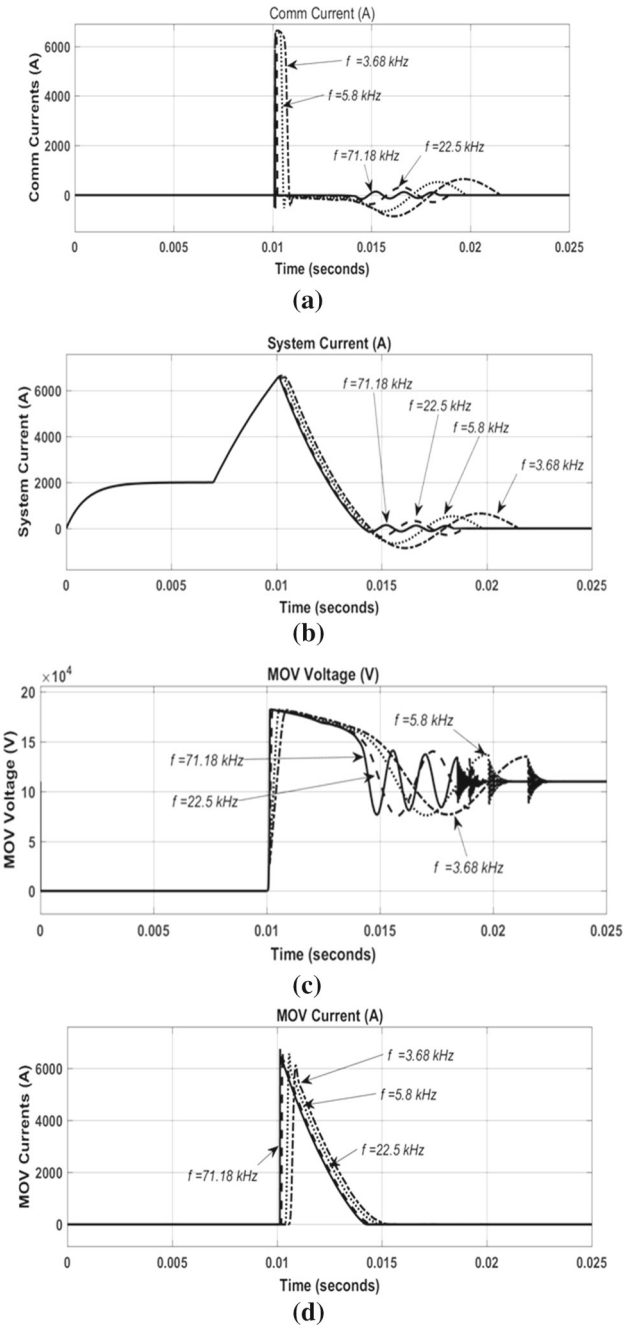

Fig. 4 Commutation current and Mov voltage and current versus time with different commutation frequencies, **a** Com current, **b** the system current, **c** Mov voltage, and **d** Mov current

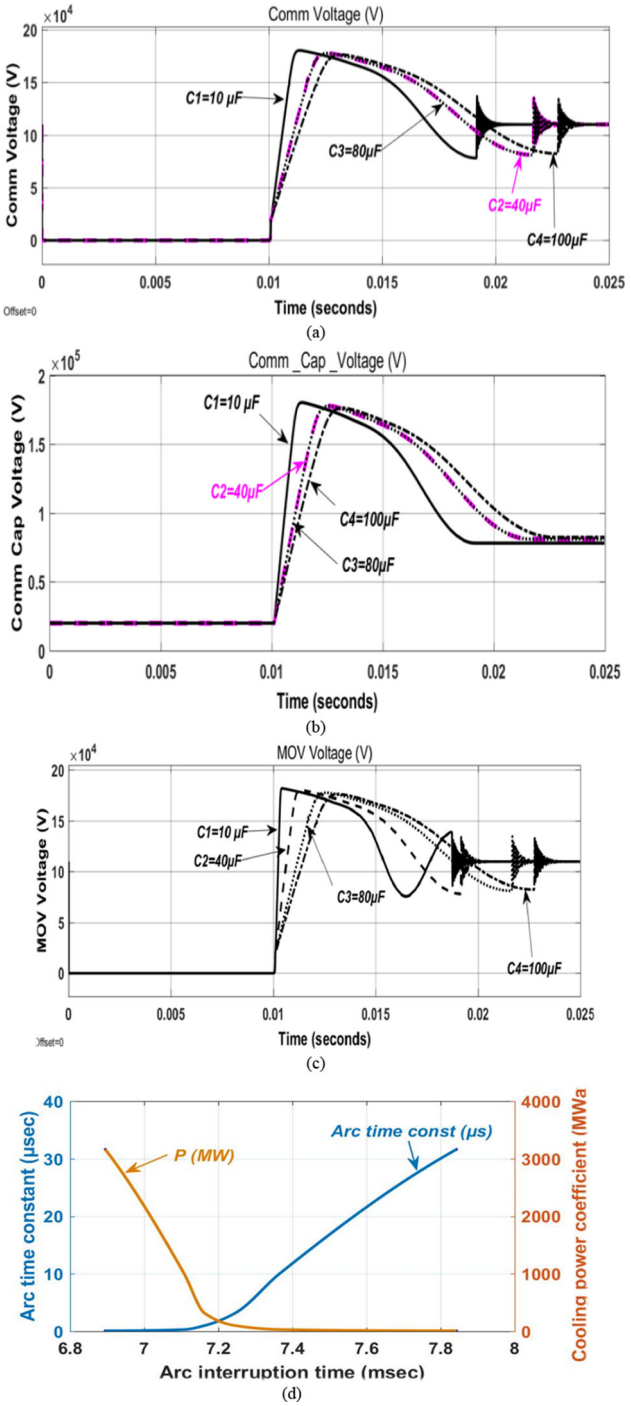

Fig. 5 TRV with different Com frequencies, Com, Com capacitor and MOV voltages in case of $L = 1$ μH versus time with different Com capacitances versus time, **a** Com, **b** Com capacitor and **c** MOV voltages, **d** effects of p and τ values on arcing time

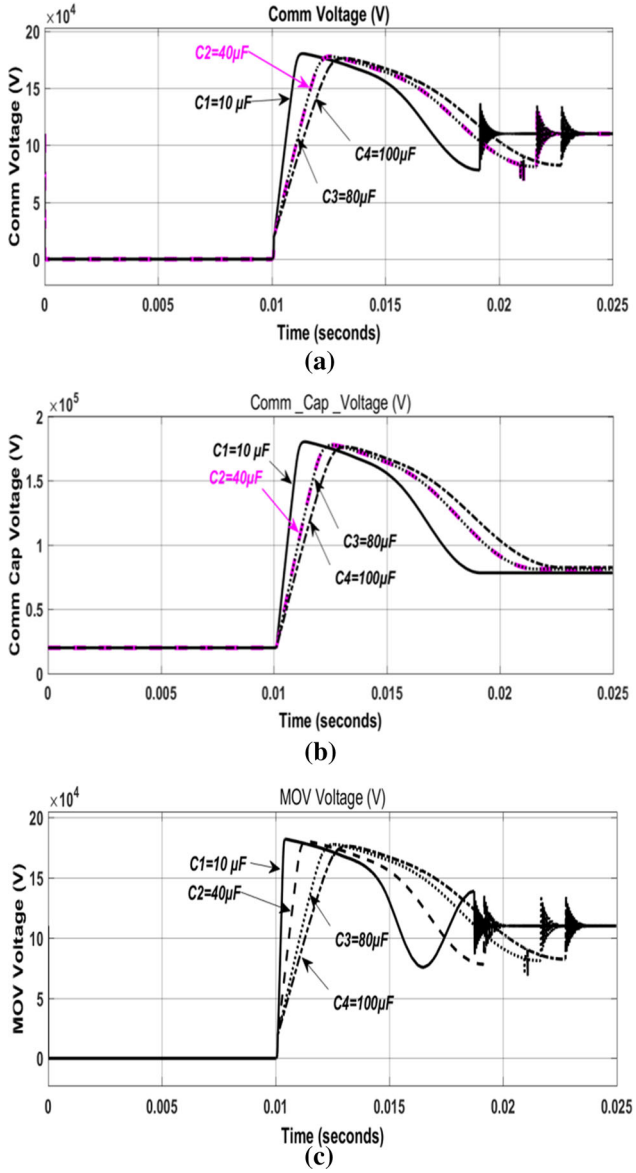

Fig. 6 Commutation, capacitor and MOV voltages in case of $L = 0.001$ μH versus time with different commutation capacitances versus time, **a** commutation, **b** Com capacitor and **c** MOV voltages

4.3 Damping resistance effect on the TRV

The high transient recovery voltage appears across the HVD-CGCB contacts having value in the order of several times the operating voltage. If this voltage is not allowed to be discharged, it may cause breakdown of the circuit-breaker insulation. To overcome this difficulty, resistance in series with capacitance switching branch is adopted and connected in shunt with the arc as shown in Fig. 1. Figure 7a shows the transient recovery voltage when the damping branch resistance R_1 is changed from 100 Ω to 1000 Ω and the capacitance is removed. As it is noticed in this figure the peak value of TRV reaches to 170 kV regardless of the resistance value. Some changes have been observed in the TRV wave forms with R_1 increases. No oscillations are noticed in these waves. When adding a capacitance of $C_1 = 5000$ pF to the damping branch, the TRV peak value is increased to 185 kV as shown in Fig. 7b. Oscillations of TRV are observed starting

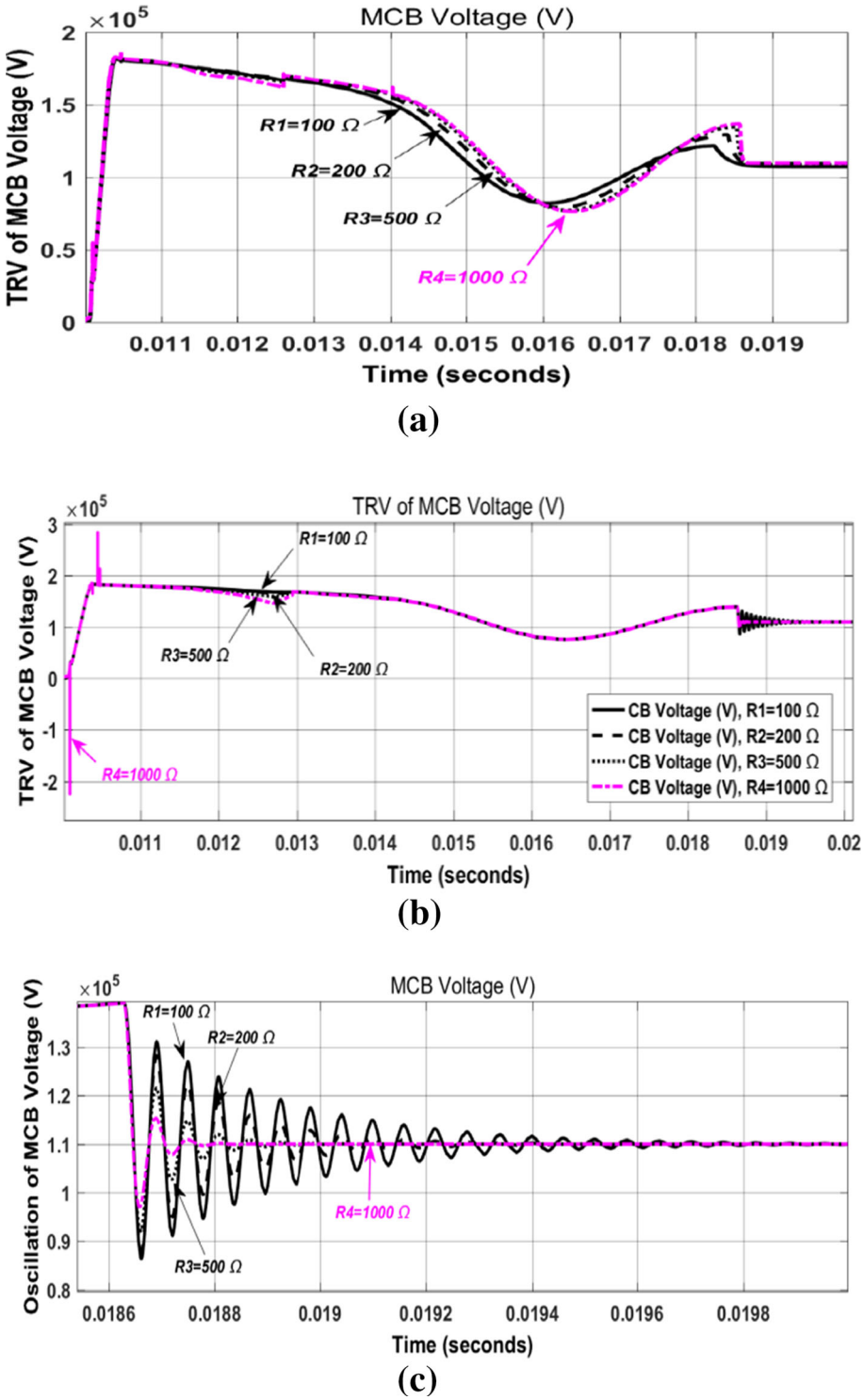

Fig. 7 Re-striking voltage versus time **a** the damping resistances changed from 100 Ω to 1000 Ω and the capacitance is removed, **b** the damping resistances changed from 100 Ω to 1000 Ω with adding the capacitance and **c** TRV oscillations

from 0.0186 ms and their peaks decrease with damping resistance increase as given in Fig. 7c. Elimination of the damping capacitance helps in reducing the TRV effects. Unfortunately it is difficult to remove the capacitive effects completely due to the presence of stray capacitance.

4.4 Simulation using Cassie's model

The HVDCGCB model given in Fig. 1 is re-utilized to simulate Cassie's model with removing the Com LC branch. As discussed in Mayr's model, the DC fault is simulated by MATLAB/Simulink as given in Fig. 8a and the system oper-

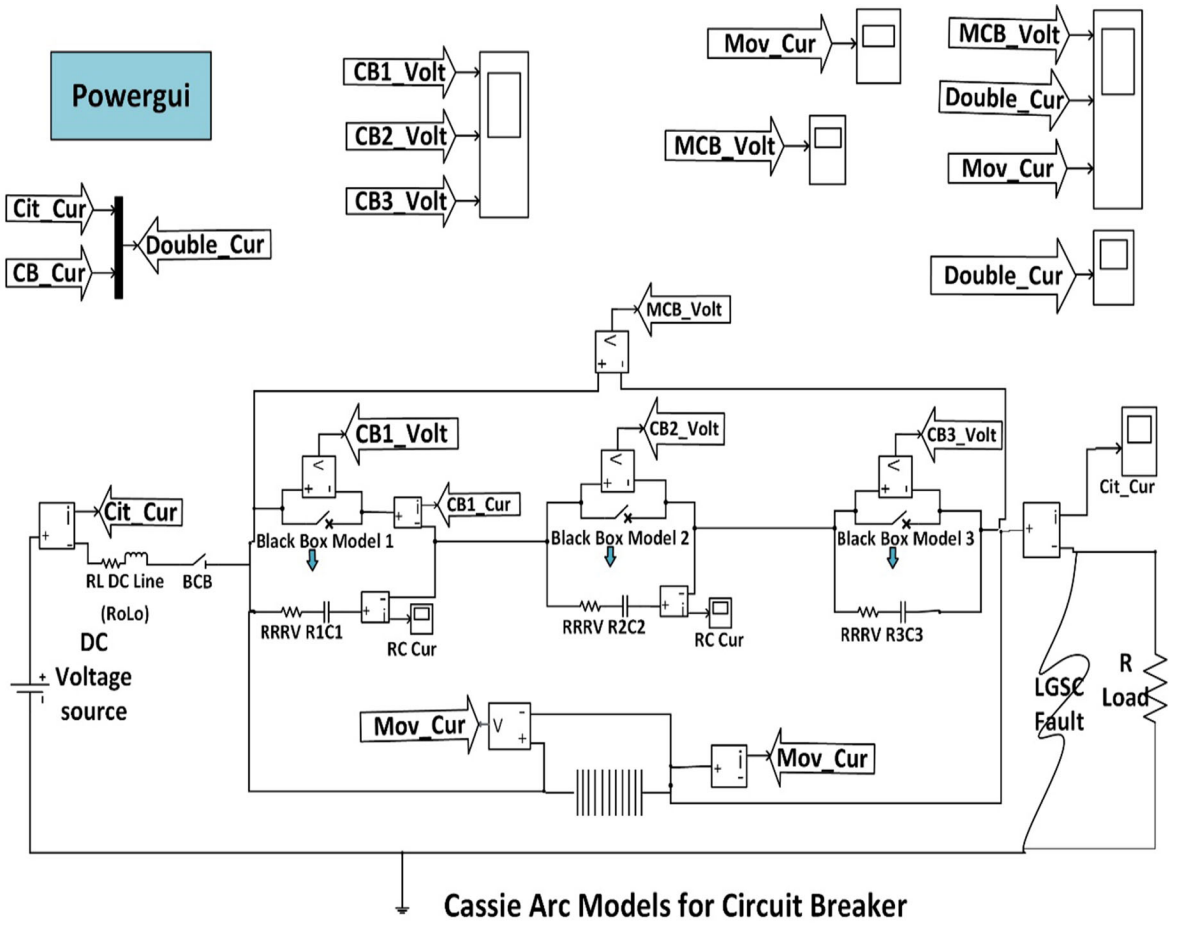

(a)

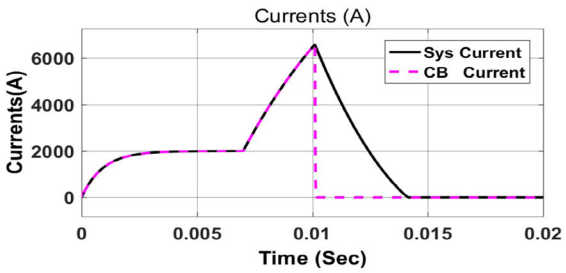

(b)

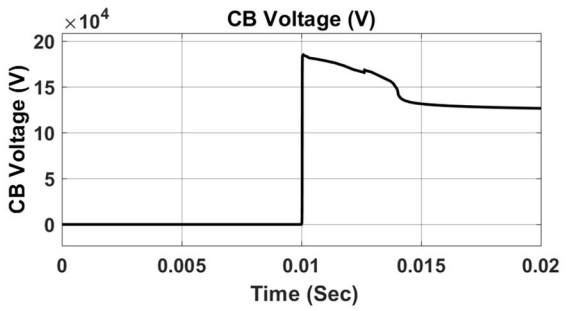

(c)

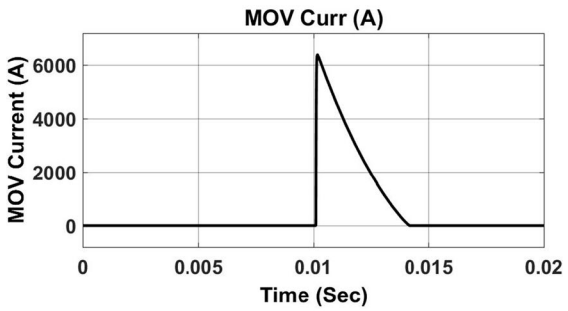

(d)

Fig. 8 MATLAB/Simulink and the simulation of the model using Cassie and the outputs of Cassie closest case, **a** MATLAB/Simulink using Cassie model, **b** CB and system currents, **c** CB voltage, **d** MOV current

Table 2 Comparison of the results obtained by Cassie and Mayer

Maximum value	I_{System} (kA)	I_{CB} (kA)	I_{MOV} (kA)	V_{CB} (kV)	Arc interruption time in ms
Cassie model	6.50	6.49	6.35	185.1	7.042
Mayr model	6.60	6.714	6.673	182.7	7.24261

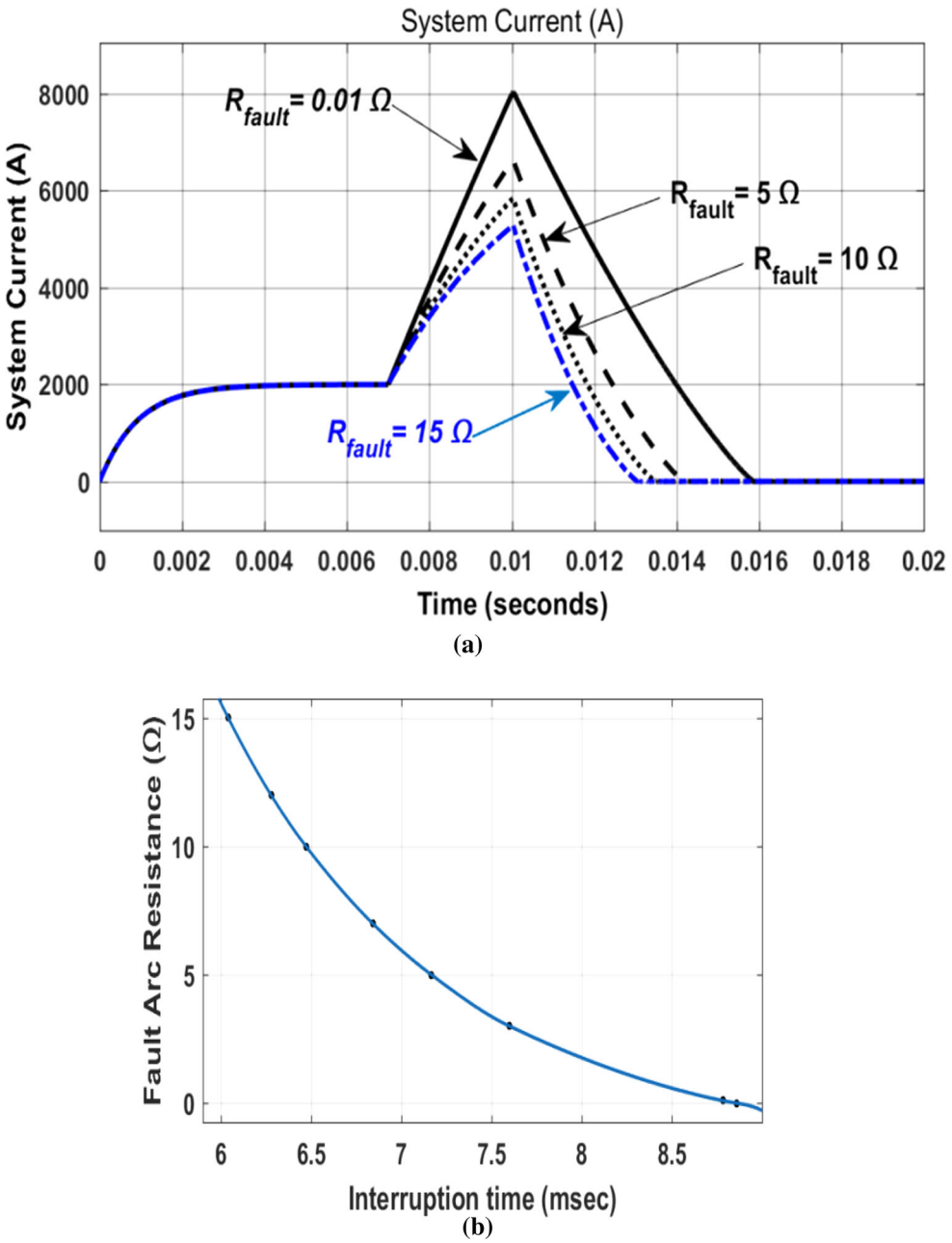

Fig. 9 Studying Cassie's model responses for changing the fault arc resistance, **a** transient responses at different values of fault arc resistance, **b** effects of fault arc resistance value on arcing time using Cassie black box arc model

ation sequence of Cassie model is as done before when using Mayr's model as the following:

(1) In the Cassie BBAM, it is not required to utilize the Com LC branch in the design of the HVDC CB, while the value of the steady-state arc voltage U_C must be larger than the DC source voltage to reduce the fault

Table 3 Cassie and Mayr's BBAM parameters for simulated tests at different values R_{fault}

Fault arc resistance R_{fault} (Ω)	Arc interruption time (Mayr) (ms)	Arc interruption time (Cassie) (ms)	Difference (ms)	Max value of I_{System} (kA)	Max value of V_{CB} (kV)
0.001	9.1218	9.012	0.1098	8.243	186.2
0.01	9.1127	8.858	0.2547	8.238	186.1
1	8.4911	8.212	0.2791	7.777	185.3
3	7.8112	7.601	0.2102	7.183	184.1
5	7.3685	7.168	0.2005	6.737	183.2
8	6.9000	6.852	0.048	6.204	181.9
10	6.6643	6.473	0.1913	5.910	181.2
15	6.2346	6.042	0.1923	5.324	180.1

Table 4 Cassie and Mayr BBAM parameters for simulated tests at variant fault locations

Fault location from the HVDC source	Line fault impedance, in Ω	Interruption time in ms using Mayr model	Interruption time in ms using Cassie model	Difference in time between Mayr and Cassie in ms	Maximum value of the system current (kA)
10% line	0.1746 + j 0.00506	3.9034	3.810792	0.092608	17.16
20% line	0.3492 + j 0.01012	4.55103	4.453396	0.097634	14.93
30% line	0.5238 + j 0.01518	5.0679	4.957932	0.109968	12.80
40% line	0.6984 + j 0.02024	5.4951	5.3728192	0.122281	11.15
50% line	0.873 + j 0.0253	5.8627	5.72685	0.13585	9.905
60% line	1.0476 + j 0.03036	6.1881	6.03901	0.14909	8.938
70% line	1.2222 + j 0.03542	6.483	6.32096	0.16204	8.170
80% line	1.3968 + j 0.04048	7.0444	6.57944	0.46496	7.082
90% line	1.5714 + j 0.04554	7.00565	6.819517	0.186133	7.032
100% line	1.746 + j 0.0506	7.2429	7.04585	0.19705	6.599

current value in the circuit to zero rapidly, if this is not happened, the MCB could not successfully interrupt the arc.

(2) Once the MCB current decreases to zero, the arc extinguishes and TRV happens.

(3) The TRV between the MCB contacts is still increasing until reaching to the MOV protection voltage level. Consequently, the current initiates to grow in the MOV branch.

(4) The residual energy in the system inductances is absorbed by the arrester. Since this energy is totally absorbed, the LGSCF is interrupted.

(5) It is interesting to know the best performance of Cassie BBAM in the high current period of the arc as it relies on convection loss in this region; consequently the Cassie BBAM is not suitable for the near of the current zero crossing.

A lot of calculations are done using different values of Cassie parameters. Cassie parameters $\tau = 100 \times 10^{-7.5}$ s, $U_C = 160$ kV, $R_1 = 200\ \Omega$, $C_1 = 115$ nF and BCB exists and separates at 14 ms proved to be good simulation to the HVDCGCB. The outputs are shown in Fig. 8, and the main comparison between the results of Cassie and Mayr models comparison results is given in Table 2.

From this table it is noticed that Cassie and Mayr models give very close values of the system current, CB current, Mov current, arc interruption time and transient recovery voltage. Slight differences are noticed between Cassie and Mayr calculations.

The results given in Fig. 8 proved that in Cassie model there is no need for using resonance LC circuit connected in parallel with the HVDCGCBs, while the value of the steady-state CB voltage is over than the supply voltage, this decreases the value of fault current to reach zero quickly as shown clearly in Fig. 8a, b; otherwise the breaker cannot effectively interrupt the fault current.

It is noticed also that, during the interval time near current zero crossing, not only the arc current is reduced, but also the current begins to flow through the MOV branch. The MOV starts to absorb the rest energy in the system inductances. As soon as the MOV absorbs this energy in 4 ms time period and the LGSCF is removed.

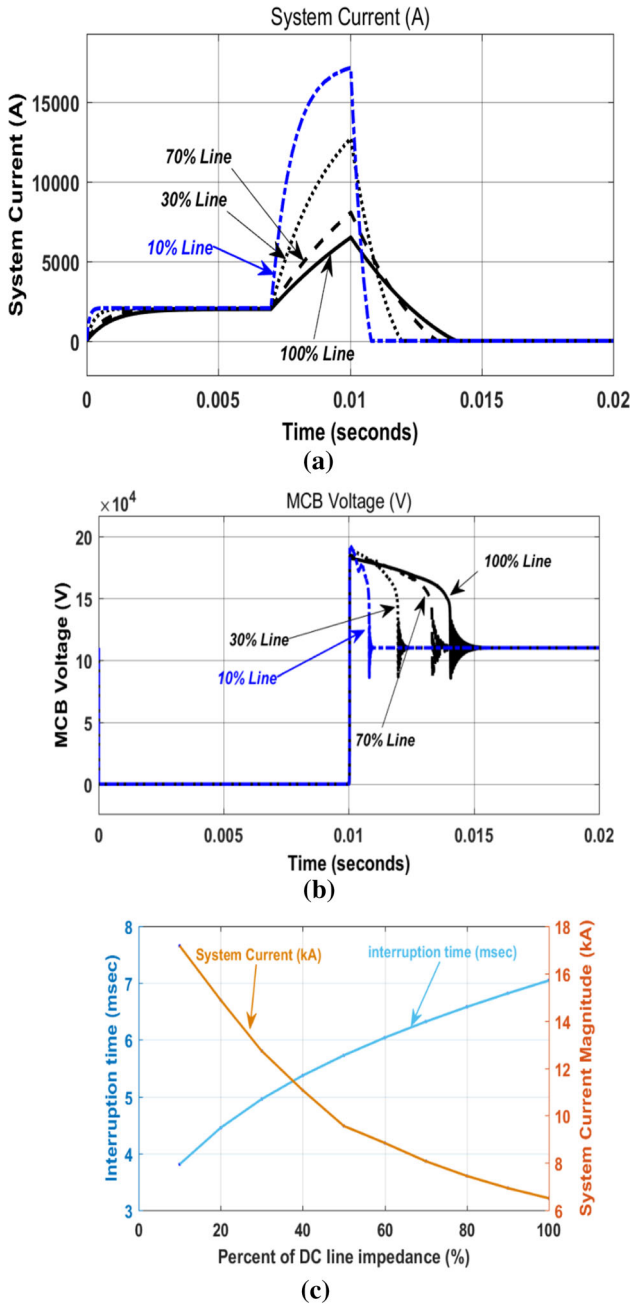

Fig. 10 Cassie outputs at different line cases considering high-voltage source side as reference in fault location measurements **a** system current, **b** MCB voltage and **c** the relation between the fault locations verses the interrupting time and system current magnitude in kA

5 Un-controlled parameters affecting the arcing time of HVDCGCBs

5.1 The change of the fault arc resistance

According to [42, 43] the minimal value of the arc fault resistance for line-to-ground faults is lower than 0.1 Ω for the fault current in the range of 1 kA to 10 kA, while the maximal value of fault resistance is 10 Ω for instantaneous protections, and 15 Ω for delayed protections. The change of the fault arc resistance is uncontrolled parameter.

Comprehensive simulations are done to study the impact of changing the fault resistance (from less than 0.1 to 15 Ω) on the interruption time of the HVDC CB as presented in Fig. 9a. From this figure it is noticed that any increase in the fault resistance implies to a decrease in the arc interruption time which means rapid arc interruption and less magnitudes of the system arc current. This of course because the high value of fault resistance aiding in reducing the arc current to be less value, however, the voltage of arc rises rapidly obliging the current to reduce rapidly to zero. But for the lower values of fault resistance, the fault current rises quickly and the voltage of arc reduces, and the interrupter requires a long time to interrupt the arc current. The impact of the changing of fault resistance value on arcing time is introduced in Fig. 9b using Cassie and Mayr black box arc model. It is observed that the arcing time decreases from 8.05 ms at 0.01 Ω (the minimal value of fault resistance) to 7.168 and 6.042 ms when the fault resistance value is raised to 5 and 15 Ω respectively.

Table 3 gives the fault arc resistance effect on the arcing time using Cassie and Mayr's black box arc models. As shown in this table the difference in the interrupting time is in the range between 1.2% and 3%. This is referring to the considered assumptions of each model.

5.2 The change of the fault location on the DC line

The HVDC circuit breaker model given in Fig. 1 is modified to protect the short transmission line 50 km long, 110 kV; its total resistance is 1.746 Ω and its total inductance is 50.6 mH. This line is used in feeding 2 kA resistive load. The fault impedance of the HVDC transmission line plays an important factor in the circuit breaker interrupting time. So, if the fault occurs far away the sending end point and near to the load, the value of the fault impedance seen by the circuit breaker employed for 50 km transmission line protection increases, consequently the fault current decreases and the interrupting time of the circuit breaker near the HVDC source increases. Otherwise, if the fault occurs near to the HVDC sending end, the value of the fault impedance decreases and an increase in the fault current will be happened and the time for fault interruption decreases.

Table 4 shows the influence of varying the fault location that is measured from the HVDC source, on the interruption time of the arc using Cassie and Mayr black box arc models. It confirms that the interruption time of the arc is increased from 3.810792 ms for a fault occurring at 10% of the line to only 7.045 ms if the fault is located at 100% of the line as shown in Fig. 10a using Cassie's BBAM parameters. Similar results are obtained using Mayr model as given in the same table. The difference between the two models is in the range

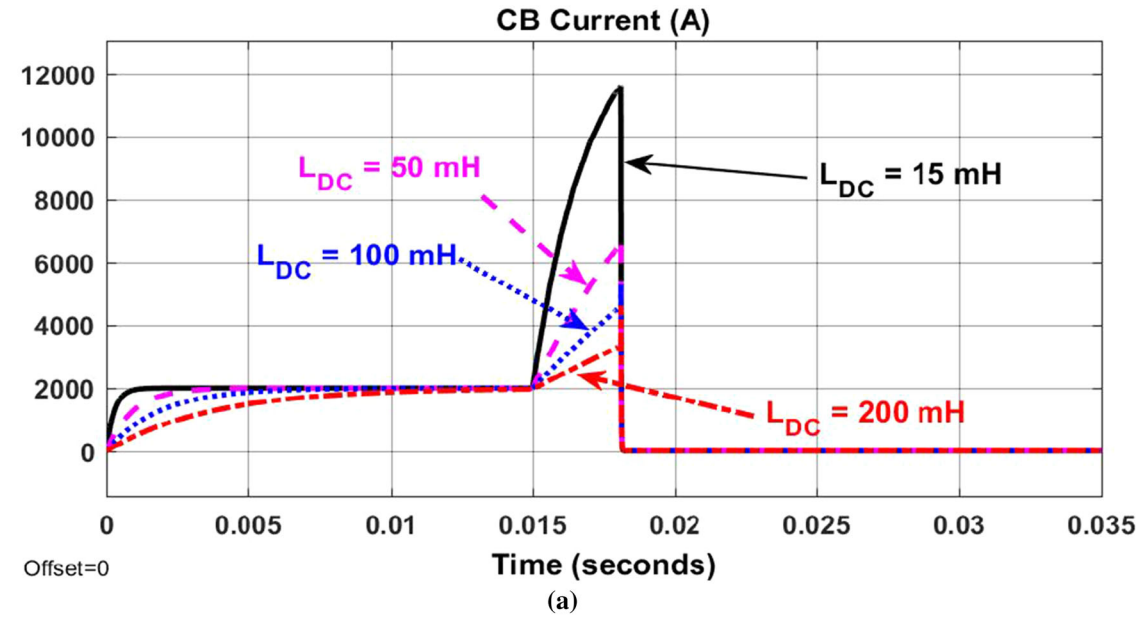

(a)

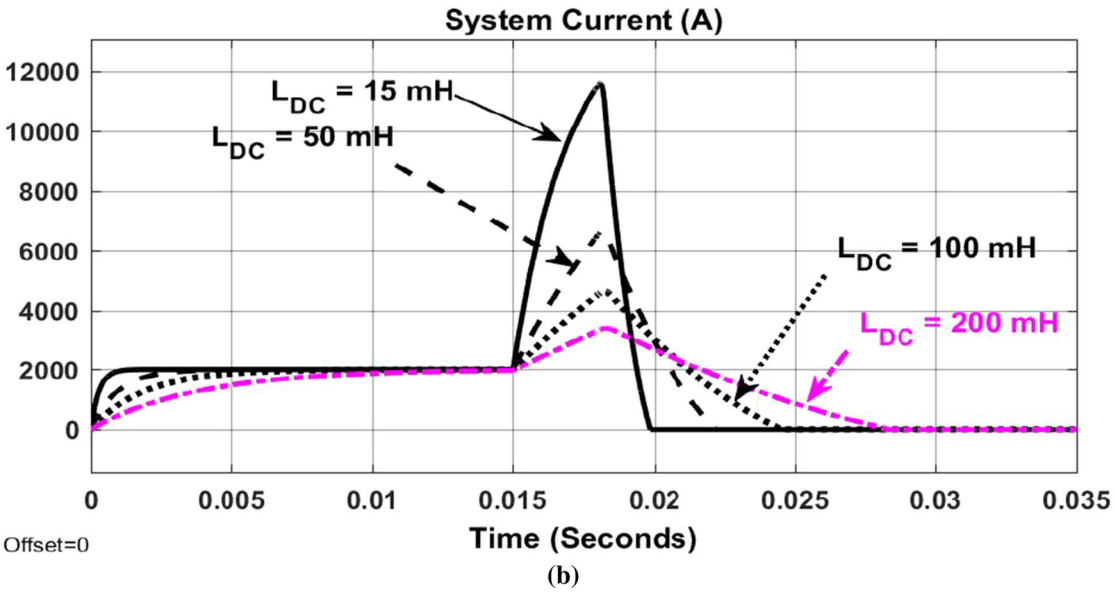

(b)

Fig. 11 The interrupting currents at different values of DC inductance, **b** CB current, **a** system current

of 2.3% to 2.6%. This may be due to the assumptions of Mayr and Cassie's models.

Slight decrease in the transient recovery voltage and its staying to longer time with remarkable oscillations in case of increasing the fault location along the transmission line are shown in Fig. 10b. The magnitude of the system fault current increases when the fault occurs near to the HVDC source point and vice versa as presented in Fig. 10c. The interruption time decreases when the fault occurs near to the source point and vice versa and this is shown in Fig. 10c. This infers that when the fault occurs far away the source point, the transmission line fault impedance value is regarded as a portion of the transient impedance of the fault increases, so the current of the fault decreases and consequently the arc interruption time increases, and vice versa. That is in agreement with that mentioned by Lee et al. [44].

To study the circuit breaker performance with the increase in the transmission line inductance (L_{DC}), its inductance is changed to be 15 mH, 50 mH, 100 mH and 200 mH. Figure 11a shows the circuit breaker interrupting current and time at different values of (L_{DC}). It is observed that the interrupting current decreases with the increase in transmission line inductance (L_{DC}); while the interrupting time remains constant, there is an intersection point at the peak values of the circuit breaker current. This may be due to that the steady-state voltage of CB is over than the supply voltage

Table 5 The relation between the energy absorbed by the DCCB system (E) versus the line inductance and the time required to dissipate this energy

Energy absorbed in kJ	Transmission line inductance in mH	Time to dissipate the stored energy in ms
991.875	15	1.854
930.25	50	4.425
924.5	100	6.539
9150	200	10.368

which decreases the fault current to reach zero very quickly regardless the fault current value. After interrupting the arc current, some time passes until the network current reaches zero as given in Fig. 11b. This is due to the dissipation of the stored energy in the transmission line. It is observed that the time of the network current to reach zero increases with the increase in the (L_{DC}) value.

The instantaneous value of the energy absorbed in the DCCB system after the current is clear versus the transmission line inductance (L_{DC}), can be calculated by the relation

$$E = 0.5(i)^2 L_{DC} \tag{10}$$

From Table 5 it is noticed that the stored energy decreases with the inductance increase, while the required time to dissipation increases.

6 Conclusions

Employing BBAM models has proved more flexibility to study the effect of different controlled and uncontrolled parameters of the multi-break HVDCGCB arcing time. From the investigated forty cases done to check Mayr's model validity of the HVDC CD simulation, it is found that the optimum values of cooling factor P and arc time constant τ which give acceptable outputs are at $\tau = 10^{-6}$ s, and P in the range of 10^7 W to 10^{11} W. The output of the case $\tau = 10^{-6}$ s, $P = 10^{10}$ W, which is introduced in the article has been proved. When τ reached to 10^{-7} s, the MOV current rises and drops and thereafter rises and gradually decreases and this may lead to CB failure. Commutation parameters influence on the interrupter performance is investigated and proved good simulation of the gaseous circuit breaker interrupter. Commutation parameters influence on the interrupter performance is investigated and proved good simulation of the gaseous circuit breaker interrupter.

The frequency of the commutation current plays an influential role in the performance of the commutation switch. If the commutation current is too high, the rate of change in current with time (di/dtl) near the current zero might be too large, which may lead to the failure of interruption. Using Cassie's model proved good simulation of HVDCGCB, when the steady-state value of CB voltage is over than the supply voltage, this decreases the value of fault current to reach zero quickly. It is also concluded that the fault site on the transmission line plays an important factor in influencing the HVDC circuit breakers arcing time and transient recovery voltage, as slight decrease in the peak value of the transient recovery voltage and its staying to longer time with remarkable oscillations in case of increasing the fault location along the transmission line is observed. The interruption time decreases when the fault occurs near to the source point and vice versa.

Finally, as it is known SF_6 gas has better behavior than vacuum because it has high dielectric strength and it is used as quenching medium. The use of SF_6 gas reduces the HVDCGCB size and the number of series modules. The current zero can be easily achieved by driven oscillation because of the superior negative resistance characteristic of SF_6. Unfortunately it has environmental impacts. On the other side HVDCVCB has the rapid dielectric strength recovery speed which has the advantage of interrupting high frequency current. VDCCB is outstanding properties concerning short circuit current control. The VDCCB applications are still mostly in medium-voltage networks. Significant efforts are required to be used in high-voltage circuits.

References

1. He Z, Hu J, Lin L, Zeng R (2016) Mechanical DC circuit breakers and FBSM-based MMCs in a high-voltage MTDC network: coordinated operation for network riding through DC fault. In: International conference on renewable power generation (RPG 2015), Beijing, China
2. Lin W, Jovcic D, Nguefeu S, Saad H (2016) Modelling of high-power hybrid DC circuit breaker for grid-level studies. IET Power Electron 9:237–246
3. Li G, Liang J, Balasubramaniam S et al (2017) Frontiers of DC circuit breakers in HVDC and MVDC systems. In: 2017 IEEE conference on energy internet and energy system integration (EI2), Beijing, China
4. Masaaki Komatsu M (2017) Basic evaluation for the DC7 circuit breaker using power semiconductor with fault current limiting feature. In: 2017 IEEE international telecommunications energy conference (INTELEC), Broadbeach, QLD, Australia
5. Monadi M, Koch-Ciobotaru C, Luna A et al (2016) Multi-terminal medium voltage DC grids fault location and isolation. IET Gen Transm Distrib 10:3517–3528
6. Tahata K, El Oukaili S, Kamei K, Yoshida D, Kono Y, Yamamoto R, Ito H (2015) HVDC circuit breakers for HVDC grid applications. In: 11th IET international conference on AC and DC power transmission, Birmingham, UK
7. Jaganath K, Henry G, Karsten H, Sebastian N (2016) A modular bi-directional hybrid circuit breaker for medium- and high-voltage DC networks. In: 18th European conference on power electronics and applications (EPE'16 ECCE Europe), Karlsruhe, Germany

8. Koldby E, Hyttinen M (2009) Challenges on the road to an offshore HVDC grid. In: Nordic wind power conference, Bornholm, Denmark, 10–11 Sept 2009
9. Mokhberdoran A, Carvalho A, Leite H, Silva N (2014) A review on HVDC circuit breakers. In: 3rd renewable power generation conference (RPG 2014), Naples
10. Andersson S, Henriksson A (2001) Passive and active dc breakers in the three Gorges-Changzhou HVDC project. B.Sc.E.E, ABB
11. Leterme W, Van Hertem D (2015) Classifcation of fault clearing strategies for HVDC grids. In: Cigre Lund symposium, Lund
12. Lars L, Magnus E, Lars J et al (2015) Medium voltage DC vacuum circuit breaker. In: 3rd international conference on electric power equipment—switching technology (ICEPE-ST), Busan, South Korea, Oct 2015
13. Xiang B, Zhang L, Yang K, Tan Y, Liu Z, Geng Y, Wang J, Yanabu S (2016) Arcing time of a DC circuit breaker based on a superconducting current-limiting technology. IEEE Trans Appl Supercond 26(7):1–5
14. May TW, Yeap YM, Ukil A (2016) Comparative evaluation of power loss in HVAC and HVDC transmission systems. In: 2016 IEEE region 10 conference (TENCON), Singapore
15. Belda NA, Smeets RPP (2017) Test circuits for HVDC circuit breakers. IEEE Trans Power Deliv 32:285–293
16. Darwish HA, Izzularab MA, Elkalashy NI (2006) Enhanced commutation circuit design of HVDC circuit breaker using EMTP. In: 2005/2006 IEEE/PES transmission and distribution conference and exhibition, Dallas, TX, USA
17. Gouda OE, Ibrahim DK, Soliman A (2019) Parameters affecting the arcing time of HVDC circuit breakers using black box arc model. IET Gener Transm Distrib 13:461–467
18. Wang W, Li Y, Wu X, Zhang X (2019) A novel solid-state circuit breaker for on-board DC micro grid system. IEEE Trans Power Electron 66(7):5715–5723
19. Win Y, Rong M, Yang F (2019) Development of a novel HVDC circuit breaker combining liquid metal load commutation switch and two-stage commutation circuit. IEEE Trans Power Electron 66(8):6055–6064
20. Zhang X, Yu Z, Chen Z, Huang Y, Zhao B, Zeng R (2019) Modular design methodology of DC breaker based on discrete metal oxide varistors with series power electronic devices for HVDC application. IEEE Trans Power Electron 66(10):7653–7662
21. Xiang B, Gao L, Luo J, Wang C, Nan Z, Liu Z, Geng Y, Wang J, Yanabu S (2019) A CO_2/O_2 mixed gas DC circuit breaker with superconducting fault current-limiting technology. IEEE Trans Power Deliv 35:1960–1967
22. Zha W, Qiu Q et al (2020) Quench and recovery characteristics of solenoid and pancake superconducting fault current limiter (SFCL) under DC impact current. IEEE Trans Appl Supercond 30(3):1–5
23. Wang Y, Bi Z, Zou J, Huang Z, Dong W (2017) Investigation on the interrupting test of mechanical HVDC vacuum circuit breaker. In: 2017 4th international conference on electric power equipment: switching technology (ICEPE-ST), Xi'an
24. Walter M, Franck C (2014) Improved method for direct black-box arc parameter determination and model validation. IEEE Trans Power Deliv 29(2):580–588
25. Elkalashy NI (2007) Modeling and detection of high impedance arcing fault in medium voltage networks. Ph.D. thesis, TKK Dissertations 95 Espoo
26. Darwish HA, Elkalashy NI (2005) Universal arc representation using EMTP. IEEE Trans Power Deliv 20(2):772–779
27. Lim S-W, Amir Khan U, Lee J-G, Lee B-W, Kim K-S, Gu C-W (2015) Simulation analysis of DC arc in circuit breaker applying with conventional black box arc model. In: 2015, 3rd international conference on electric power equipment—switching technology (ICEPE-ST), Busan
28. Zhang Y, Shi Z, Wang Q, Gao Z, Jia S, Wang L (2016) Experimental investigation on HVDC vacuum circuit breaker based on artificial current zero. In: 2016 27th international symposium on discharges and electrical insulation in vacuum (ISDEIV), Suzhou
29. Shi ZQ, Zhang YK, Jia SL, Song XC, Wang LJ, Chen M (2015) Design and numerical investigation of A HVDC vacuum switch based on artificial current zero. IEEE Trans Dielectr Electr Insul 22:135–141
30. Qin T, Dong E, Liu G, Zou J (2016) Recovery of dielectric strength after dc interruption in vacuum. IEEE Trans Dielectr Electr Insul 23(1):29–34
31. Song X, Peng C, Huang AQ (2017) A medium voltage hybrid DC Circuit breaker part I: solid state main breaker based on 15 kV SiC emitter turn-of (ETO) thyristor. IEEE J Emerg Sel Top Power Electron 5:278–288
32. Li R, Wang ZX, Holliday D, Yao LZ, Williams BW (2016) DC circuit breaker requirements in multi-terminal HVDC systems. In: 8th IET international conference on power electronics, machines and drives (PEMD 2016), Glasgow
33. Eriksson T, Backman M, Halln S (2014) A low loss mechanical HVDC breaker for HVDC grid application. In: B4-303, Paris
34. Kim BC, Chung YH, Hwang HD, Mok HS (2015) Development of HVDC circuit breaker with fast interruption speed. In: 2015 9th international conference on power electronics and ECCE Asia (ICPE-ECCE Asia), Seoul, South Korea, pp 2844–2848
35. Wang Q, Shi Z, Zhang Y, Jia S, Wang L (2016) Simulation and analysis of A HVDC vacuum circuit breaker based on artificial current zero. In: 2016 27th international symposium on discharges and electrical insulation in vacuum (ISDEIV), Suzhou
36. Liu S, Liu Z, de Jesus Chavez J, Popov M (2019) Mechanical DC circuit breaker model for real time simulations. Int J Electr Power Energy Syst 107:110–119
37. Schavemaker PH, Van der Slois L (2000) An improved Mayer type arc model based on current—zero measurements. IEEE Trans Power Deliv 15(2):580–584
38. Xiang B, Ting Y, Li K, Liu Z, Wang J (2020) A novel artificial current zero SF6 Dc circuit breaker charging by superconducting voltage. Accepted to be publish in IEEE PES transactions on power delivery
39. Darwish HA, Izzularab MA, Elkalashy NI (2006) Enhanced commutation circuit design of HVDC circuit breaker using EMTP. In: 2005/2006 IEEE/PES transmission and distribution conference and exhibition
40. Bizzarri F, Brambilla A, Gruosso G, Gajani GS, Bonaconsa M, Viaro F (2017) A new black-box model of SF 6 breaker for medium voltage applications. In: IECON 2017-43rd annual conference of the IEEE on industrial electronics society, pp 32–37
41. Park KH, Lee HY, Asif M, Lee BW, Shin TY, Gu CW (2017) Assessment of various kinds of AC black-box arc models for DC circuit breaker. In: 2017 4th international conference on electric power equipment-switching technology (ICEPE-ST), pp 465–469
42. Franck CM (2011) HVDC circuit breakers: a review identifying future research needs. IEEE Trans Power Deliv 26(2):998–1007
43. De Andra V, Somentino E (2011) Typical expected values of the fault resistance in power system. In: IEEE/PES transmission and distribution conference and exposition: Latin America (T&DLA), Sao Paulo, Brazil, Nov 2010, pp 602–609
44. Lee LH, Asif M, Park KH, Lee BW (2019) Assessment of appropriate SFCL type considering DC fault interruption in full bridge modular multilevel converter HVDC system. Phys C: Supercond Appl 563:1–6